Modeling hydrogen dragging by mobile dislocations in finite element simulations

Y. Charles, Jonathan Mougenot, Monique Gasperini

Modeling hydrogen dragging by mobile dislocations in Finite Element simulations

Yann CHARLES[1], Jonathan MOUGENOT, Monique GASPERINI

Université Sorbonne Paris Nord, Laboratoire des Sciences des Procédés et des Matériaux, LSPM, CNRS, UPR 3407, F-93430, Villetaneuse, France

Abstract

Finite element simulation modeling permits to predict hydrogen concentration for various initial boundary-values problems, but the results depend on the underlying transport mechanisms accounted for. Trapping process is a key factor in the apparent hydrogen diffusion, and the case of mobile traps as dislocations needs modification of the hydrogen transport equation usually considered in the literature. An extension of this model is proposed where hydrogen dragging by mobile traps is modeled by reaction-diffusion equations, involving trapping and detrapping kinetic, and is applied for evolving trap density with plastic strain. The consequences of trapped hydrogen mobility on diffusive hydrogen repartition in a reference Small Scale Yielding configuration are focused on, especially in term of acceleration of hydrogen transport. The potentiality of the model is illustrated by the modeling of the trapped hydrogen breakaway from fast moving dislocations.

keywords: Hydrogen diffusion, Trapping, Finite elements calculations, dislocations

1 Introduction

Hydrogen embrittlement is a severe risk of early failure for metallic structures under hydrogen environment, and its prevention is essential to guarantee the safety of installations and equipment and thus constitutes an essential step for the development of the hydrogen energy sector. The hydrogen storage and supply means (pipelines, tanks…) involve shaping operations by plastic deformation in their qualification procedure [1,2]. Prediction of hydrogen concentration in the material and its evolution with plastic deformation is a prerequisite for the prevention of hydrogen embrittlement and needs to solve initial-boundary value problems. In this context, finite element simulation is a powerful tool to model complex structures and their behavior in aggressive environments; however, the computations reliability highly depends on the realistic mechanisms of hydrogen-material interactions accounted for. Due to its small size, the hydrogen atom can enter into metallic materials, diffuse through the crystal lattice and be trapped by various microstructural defects (vacancies, dislocations, grains boundaries…). As many scales are involved in hydrogen transport from the atomic scale [3] to the macroscopic one [4], phenomenological description of hydrogen transport mechanisms in the frame of continuum mechanics is a good compromise to access mechanical and hydrogen concentration and has been used by several authors to limit computational cost in finite element simulations (see, e.g., [5-7]).

In pioneering works, hydrogen transport including lattice diffusion and trapping by dislocations was accounted for in finite element models using the equation proposed by Kumnick et al. [8],

[1] Corresponding author, yann.charles@univ-paris13.fr, LSPM-CNRS, Université Sorbonne Paris Nord, 99 avenue Jean-Baptiste Clément, F-93320 Villetaneuse, France

modified by Sofronis [9,10] and by Krom [11]. In this model, the mobility of traps is not considered. The hydrogen concentration is defined by its volumetric concentration $C = C_L + C_T$ where C_L and C_T are respectively the diffusive part and the trapped part. Only one type of trap is considered, namely the trapping by dislocations, through the trap density N_T [10,12] which evolves with the equivalent plastic strain $\bar{\varepsilon}_p$.. C_T and N_T are linked by the trap occupancy θ_L ($\in [0,1]$): $C_T = N_T\theta_T$, while $C_L$is linked to the normal interstitial lattice sites (NILS) density N_L by the lattice site occupancy θ_L ($\in [0,1]$): $C_L = N_L\theta_L$.

The diffusive hydrogen flux $\boldsymbol{\varphi}_L$, modified to account for the effect of hydrostatic pressure [10,13-15] is written as

$$\boldsymbol{\varphi}_L = -D_L\boldsymbol{\nabla}C_L - D_L C_L\frac{V_H}{RT}\boldsymbol{\nabla}P_H \tag{1}$$

where D_L is the hydrogen diffusion coefficient, R the perfect gas constant, T the absolute temperature, V_H the partial molar volume of hydrogen in solid solution and P_H the hydrostatic pressure, equal to $-1/3\ \mathrm{tr}\ \boldsymbol{\sigma}$. From mass conservation, the hydrogen transport equation can be written as

$$\frac{\partial C_L}{\partial t} + \frac{\partial C_T}{\partial t} = \boldsymbol{\nabla}.\left(D_L\boldsymbol{\nabla}C_L + D_L C_L\frac{V_H}{RT}\boldsymbol{\nabla}P_H\right) \tag{2}$$

In equation (2), the effect of trapping on hydrogen transport is expressed through the temporal evolution of C_T. The trapped hydrogen concentration can evolve either by trapping of diffusive hydrogen on available trapped sites, or because detrapping occurs towards available diffusive sites. Defining the free trapping site density N_T^* ($N_T = C_T + N_T^*$) and the free lattice sites density N_L^* ($N_L = C_L + N_L^*$), the trapping process can be written as a chemical reaction [16]

$$C_L + N_T^* \leftrightharpoons C_T + N_L^* \tag{3}$$

By assuming, following McNabb and Foster [17], a first-order chemical reaction, and that $N_L \gg C_L$ (i.e., $N_L \approx N_L^*$, or $\theta_L \ll 1$, which is a common approximation in the context of plasticity), $\partial C_T/\partial t$ can be written as [18]

$$\frac{\partial C_T}{\partial t} = \frac{k}{N_L}C_L(N_T - C_T) - pC_T \tag{4}$$

where k/N_L and p/N_L are the forward and reverse reaction rates constants. If a constant trap density N_T is furthermore assumed, equation (4) can be rewritten as

$$\frac{\partial \theta_T}{\partial t} = k\theta_L(1 - \theta_T) - p\theta_T \tag{5}$$

Oriani [19] has proposed to write the steady state solution of equation (5) as

$$K_T\theta_L = \frac{\theta_T}{1 - \theta_T} \tag{6}$$

where $K_T = k/p = e^{-\Delta E_T/RT}$is the equilibrium constant for equation (5). ΔE_T is the trap binding energy with respect to the lattice site, R the universal gas constant and T the absolute temperature.

Based on thermodynamic equilibrium between diffuse and trapped hydrogen concentrations, this approach simply considers the increase of trapping with plastic strain, without considering specific interactions between hydrogen and dislocations during plastic straining such as hydrogen transport by mobile dislocation [20].

It is indeed showed by experimental works [21-26] that hydrogen trapped near dislocations can diffuse be transported by dislocations motion, inducing a faster hydrogen transport when the dislocation velocity is higher than hydrogen diffusion rate. This hydrogen transport mechanism is then expected to significantly modify the occurrence and kinetics of material-hydrogen interactions and hydrogen embrittlement, and it has to be accounted for in the simulation of hydrogen transport. Conversely, hydrogen affects the dislocation glide velocity [27].

Few models of hydrogen transport by mobile traps can be found in the literature. In the specific case of dislocation, an analytical expression of the maximum hydrogen penetration depth as a function of material properties and the strain rate was proposed [20]. An hydrogen transport equation has been proposed by [26], including both mobile and fixed traps. Hydrogen dragging by mobile dislocation is modeled by considering a source term for diffusive hydrogen, assuming a constant dislocation density and an instantaneous. [28] proposed to describe hydrogen dragging by a trapped hydrogen flux term depending on the strain rate and on the local trapped hydrogen concentration. No global hydrogen transport equation has been expressed from this proposition. Dadfarnia and al. [29] proposed to account for hydrogen dragging by a diffusive hydrogen flux $\boldsymbol{\varphi}_d$ term depending on strain rate, mobile trap density and trap occupancy, and a given transport direction $\boldsymbol{v}_d$ (in the same manner than in the work of [30], dealing with Cottrell atmosphere stability around a mobile dislocation)

$$\boldsymbol{\varphi}_d = \theta_T N_T \boldsymbol{v}_d \tag{7}$$

They add this term in the Sofronis and McMeeking hydrogen flux [10]:

$$\boldsymbol{\varphi}_L = -D_L \boldsymbol{\nabla} C_L - D_L C_L \frac{V_H}{RT} \boldsymbol{\nabla} P_H + \theta_T N_T \boldsymbol{v}_d \tag{8}$$

(considering in equation (8) that all traps are assumed to be mobile). This approach was applied to the simulation of hydrogen repartition ahead a crack tip in small scale yielding with isotropic elastoplastic material, as in previous works [10,11,31], they showed through a parametric study the effect of the hydrogen transport by dislocation both for bcc and fcc materials, which permits to improve the simulation of hydrogen transport. This approach has been extended to crystal plasticity scale [32,33] to add the influence of polycrystalline texture on the overall hydrogen transport.

The model presented in equation (8) is based on the Oriani's assumption (equation (6)), for which a direct relationship between C_L and C_T can be defined at each time and material point: to a trapped hydrogen flux corresponds a diffusive hydrogen flux, and reciprocally. This approach, however, does not explicitly model trap mobility. From the author knowledge, no hydrogen transport equation accounting for trap mobility and trapped hydrogen dragging by mobile dislocations has been proposed in the literature. This is also the case for any other trap kind, as, e.g., vacancies and vacancy clusters. It is worth, however, to point out the work of Ebihara et al., which have modelled vacancy mobility and clustering [34], but without any consideration on trapped hydrogen dragging.

This paper aims to propose a generalization of the hydrogen transport equation, accounting for both trap mobility and hydrogen dragging by mobile traps. Noting the proposed strategy can be applied regardless of the kind of trap, it is applied in the present study on hydrogen dragging by mobile dislocations phenomenon, using simplification assumptions.

First, the modeling approach is described as well as the implementation in the Abaqus Finite Element software. An application is made on a simple configuration to point out the differences between the present approach and the more recent one proposed in the literature [29]. Using a Small-Scale Yielding (SSY) configuration, the proposed model approach is first validated for a case without no trap mobility (by comparison with already published results). Then, a parametric study is conducted to illustrate the effects of trapped hydrogen dragging by mobile

traps on hydrogen repartition, as a function of the trapping kinetic, the loading rate and the trap motion. Last, an application of the dislocation breakaway from the Cottrell atmosphere is conducted.

In the following, α-iron is considered for all applications.

2 Diffusion, trapping and dragging by mobile traps

First, the modification of the Krom and Sofronis transport equation is presented, its numerical implementation detailed, and the main consequences on Hydrogen transport pointed out, especially regarding previous models.

2.1 Trap mobility and trapped hydrogen dragging

Hydrogen dragging by mobile dislocations is assumed to follow a 3-step process: hydrogen atoms are trapped at dislocations, then transported by traps across the sample and potentially detrapped to lattice sites, depending on the detrapping kinetics. To model this 3-step process, it is thus needed to be able to model hydrogen trapping and released, and trap mobility, plus, of course, hydrogen diffusion. Furthermore, trap mobility alters the trap repartition in the sample.

For the sake of simplicity, the following assumptions are furthermore considered:

- traps are assumed to be able to move in any direction;
- all traps are considered as being mobile ones;
- trap mobility is assumed to be unaffected by trapped hydrogen or by mechanical fields.

From these assumptions, trap mobility can be described by adapting the model proposed by [35] and developed by [36-38] in which plasticity is described using a reaction-diffusion framework on dislocation densities:

$$\frac{\partial N_T}{\partial t} = \boldsymbol{\nabla}.(D_T \boldsymbol{\nabla} N_T) + \frac{\partial N_T^r}{\partial t} \tag{9}$$

D_T represents the trap diffusion coefficient and $\partial N_T^r/\partial t$ the trap creation, which can be rewritten as

$$\frac{\partial N_T^r}{\partial t} = \frac{dN_T}{d\bar{\varepsilon}_p}\dot{\bar{\varepsilon}}_p \tag{10}$$

D_T is so that [38,39]

$$D_T = \frac{v^2}{2c} \tag{11}$$

where c is a material parameter (set as 200 s^{-1} following [38]) and v represents the mean dislocation velocity, with [29]

$$v = \frac{\dot{\bar{\varepsilon}}_p}{\rho b} \tag{12}$$

b represents the magnitude of the Burger vector (equal to 0.248 nm for α-iron [40]) and ρ the dislocation's density such that, for bcc materials [29],

$$\rho = \frac{a}{\sqrt{2}} N_T \tag{13}$$

a is the lattice parameter (equal to 0.287 nm for α-iron [41]). From equation (11), v is rewritten as

$$v = \frac{\sqrt{2}\dot{\bar{\varepsilon}}_p}{baN_T} \tag{14}$$

and D_T as

$$D_T = \frac{1}{b^2 a^2 c} \frac{\dot{\bar{\varepsilon}}_p{}^2}{N_T \left(\bar{\varepsilon}_p\right)^2} \tag{15}$$

Trap mobility is thus modified by both strain rate and plasticity. Trapped hydrogen dragging by mobile traps mobility implies that $\partial C_T / \partial t$ is no longer describes by the McNabb and Foster equation, but by a transport one such that

$$\frac{\partial C_T}{\partial t} = \boldsymbol{\nabla}.(D_T \boldsymbol{\nabla} C_T) + \frac{\partial C_T^r}{\partial t} \tag{16}$$

Because trap mobility is assumed to be not affected by trapped hydrogen, the diffusion coefficient of N_T is used. The creation term $\partial C_T^r / \partial t$ corresponds to the trapping reaction process (equation (4)). Equation (16) corresponds to an alternative of the hydrogen flux due to drag by mobile dislocation proposed by [28].

Hydrogen transport and trapping (equations (2) and (4)) can then be replaced by the following system which accounts for trap mobility and trapped hydrogen dragging (there after referred as Transport, Trapping and Dragging equation, or TTD)

$$\begin{cases} (a)\ \dfrac{\partial C_L}{\partial t} = \boldsymbol{\nabla}.\left(D_L \boldsymbol{\nabla} C_L + D_L C_L \dfrac{V_H}{RT} \boldsymbol{\nabla} P_H\right) + \dfrac{\partial C_L^r}{\partial t} \\ (b)\ \dfrac{\partial C_T}{\partial t} = \boldsymbol{\nabla}.(D_T \boldsymbol{\nabla} C_T) + \dfrac{\partial C_T^r}{\partial t} \\ (c)\ \dfrac{\partial N_T}{\partial t} = \boldsymbol{\nabla}.(D_T \boldsymbol{\nabla} N_T) + \dfrac{dN_T}{d\bar{\varepsilon}_p} \dot{\bar{\varepsilon}}_p \\ (d)\ \dfrac{\partial C_T^r}{\partial t} = -\dfrac{\partial C_L^r}{\partial t} = \dfrac{k}{N_L} C_L (N_T - C_T) - p C_T \end{cases} \tag{17}$$

It is worth noting that, if $D_T = 0$ (e.g., for $\dot{\bar{\varepsilon}}_p = 0$ or in the case of non-mobile traps), the system (17) corresponds to the initial set of equations (2) and (4); it is therefore an extension of the transport and trapping equation, as initially proposed in [10] and later improved in [11] and [18], to account for respectively plasticity increase and transient trapping.

2.2 Implementation in FE Abaqus software

The implementation in Abaqus of the TTD system (equation (17)) is made based on User Subroutine development, following the works presented in previous studies (see [18,32,42-45] for further details). It is furthermore needed to include in Abaqus multi-diffusion capabilities following the scheme presented in [46]; all of the problems are simultaneously solved (mechanical, diffusion, trapping, dragging).

The implementation flowchart is presented in Figure 1; it is based on the 'coupled temp-displacement' scheme, using the degree of freedom (dof) 11 for C_L.

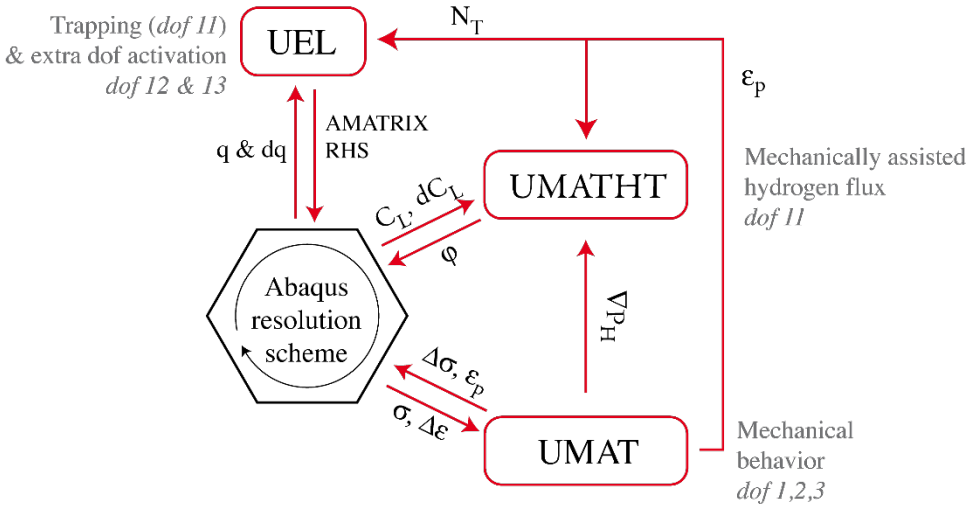

Figure 1. Implementation in Abaqus of the TTD equation.

The main features of the implementations are presented thereafter.

1. The hydrostatic pressure influence on the mobile hydrogen flux (equation (1)) is introduced using a UMATHT subroutine, being computed at each mesh integration Point and at each Newton-Raphson iteration by a UMAT one (see [42] for details), insuring a simultaneous resolution of C_L and mechanical fields. Data are transferred between User Subroutines by common blocs.
2. The resolution of C_L and mechanical fields are made based on classical finite elements (here, C3D8T).
3. Following [46], a User Element subroutine is used to
    - Activates two hidden dof (12 and 13) for C_T and N_T
    - Introduce the transport equation in the computation (equations (17)b and c), through the definition of the Abaqus vectors RHS and matrix $AMATRX$ [47]
    - Define the coupling term between C_L, C_T and N_T (equation (17)d).

The User Elements are superimposed to classical Abaqus finite elements (i.e., coupled temperature displacement ones, with 4 dof per node in 3D -numbered 1 to 3 for displacement and 11 for C_L-), and are consequently able to directly modify their formulation (Figure 2), as proved in [48].

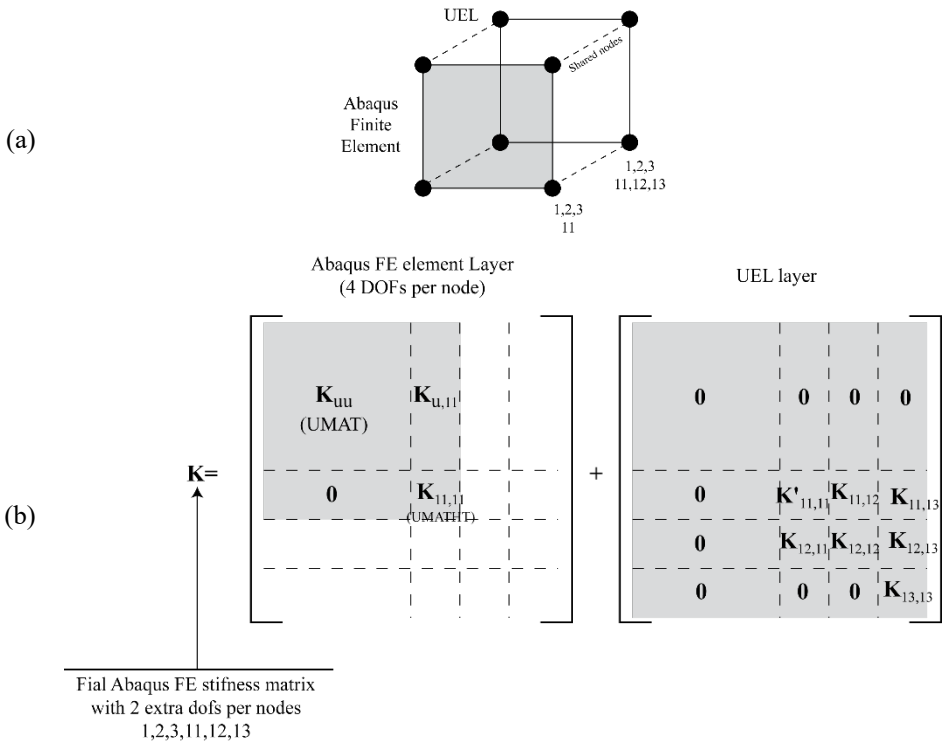

Figure 2. Principle of the UEL interaction with standard Abaqus Finite Element : (a) superposition of a UEL and an Abaqus Finite Element (with same nodes) and (b) consequences on the Abaqus Finite Element stiffness.

The superposition of an UEL and an Abaqus Finite Element leads to the modification of the stiffness matrix of the Abaqus Finite Element in several ways:

- in the current application, two dofs are automatically added by Abaqus at each node, and its global solving process account for this new problem dimension
- the Abaqus Finite Element stiffness matrix is modified by the presence of the superimposed UEL. In the present application, is added to the pure diffusion problem on C_L (dof 11, represented by equation (1)) the trapping kinetic equation in which is involved two other degree of freedom (12 and 13, equation (17)d), represented by the local stiffness matrix $\boldsymbol{K'}_{11,11}$, $\boldsymbol{K}_{11,12}$ and $\boldsymbol{K}_{11,13}$.

Last, the trap creation by plastic deformation (equation (10)) is accounted for based on common bloc, allowing the UEL to get non-converged $\bar{\varepsilon}_p$ fields during the Newton Raphson Abaqus loops.

At each Abaqus increment, all of the problems (mechanical, diffusion of hydrogen, trap mobility and hydrogen dragging) are simultaneously solved.

This scheme is a paradigm change for the resolution of hydrogen transport problem in metals: C_T and N_T shift from being internal variables defined and computed at each integration point to degrees of freedom to be determined by the Finite Element software at each node.

2.3 Consequences

The proposed modeling is based on a distinction between C_L and C_T mobilities, which interacts only through the kinetic trapping reaction given in equation (17)d.

The main consequences of the TTD equation set are:

1. no trapped hydrogen dragging can append if there is no trap ($N_T = 0$; consequently, $C_T = 0$ as well);
2. no trapped hydrogen dragging can append if there is no trapped hydrogen ($C_T = 0$);
3. trapped hydrogen movement cannot be detected in areas where C_T is homogeneous ($\boldsymbol{\nabla}.(D_T \boldsymbol{\nabla} C_T) = 0$)
4. C_L modification due to mobile trapped hydrogen is only linked to the detrapping kinetic ($\partial C_L^r / \partial t$). As a consequence, if only saturated traps are involved in the global hydrogen transport process ($\theta_T \approx 1$ everywhere), then, the C_L repartition is not affected by trap mobility. An important effect of trapped hydrogen dragging on C_L repartition can thus be obtained in a region where $\theta_T = 0$.

This last point is the most important consequence of the TTD equation set. It can be illustrated by considering a configuration in which the trapping process is initially at equilibrium (see equation (17)d): let's consider a 20 mm length bar, with a 1 mm^2 section, and meshed with 20 full integration tri-linear elements (C3D8T in Abaqus), i.e., with 8 Gauss point, representing a 1D-like configuration

The initial conditions are presented in Figure 3: C_L is constant everywhere and equal to 1, while N_T is a step function, with a maximum value equal to 0.5. Last, C_T repartition follows the N_T one, with a maximum value so that [19]

$$C_T = \frac{kC_L N_T}{pN_L + kC_L} \approx 0.499 \tag{18}$$

with, for the sake of illustration $N_L = 1\ mm^{-3}$, $k = 10\ s^{-1}$ and $p = 0.01\ s^{-1}$. Equation (18) denotes the chemical equilibrium between C_L, C_T and N_T. With this kind of configuration, trap hydrogen is always at equilibrium, either being transported by mobile traps or not.

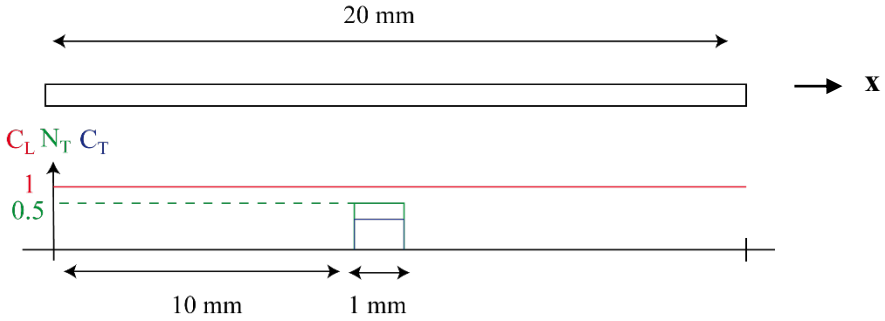

Figure 3. Initial conditions in the sample.

All the bar boundaries are considered insulated for C_L, C_T and N_T. No mechanical loadings are applied (no trap creation) and the full TTD system given in equation (17) is solved. D_T is set for the sake of illustration to 40 mm^2/s. The system evolution is presented in Figure 4.

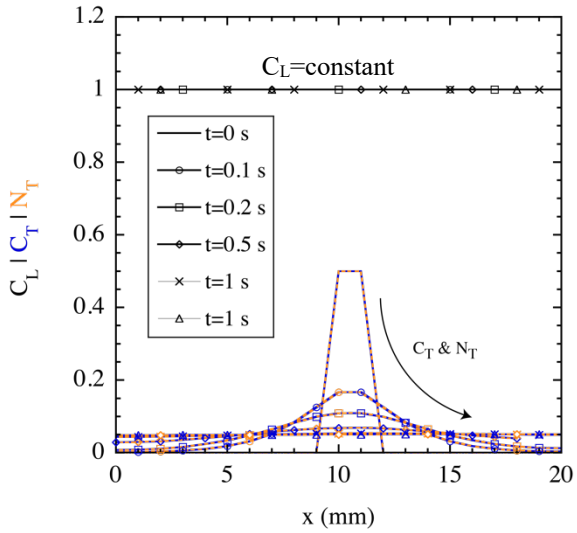

Figure 4. Repartition of C_L, C_T and N_T along the bar for different times obtained by using the TTD equation set.

It can be first observed that C_L does not depend on time: the trapping chemical reaction is as expected, at equilibrium whatever the time, and is independent on the mobility of both C_T and N_T.

The second observation is that C_T and N_T concentrations are indeed proportional whatever the time, mimicking the C_T dragging by mobile traps.

Furthermore, it can be noticed that trapped hydrogen can be mobile without any effect on the diffusive hydrogen concentration, i.e., with no effect on its flux. More generally trapped hydrogen, mobile or not, act on the mobile hydrogen concentration trough the source-like term $\partial C_L^r/\partial t$ only, and do not affect the mobile hydrogen flux.

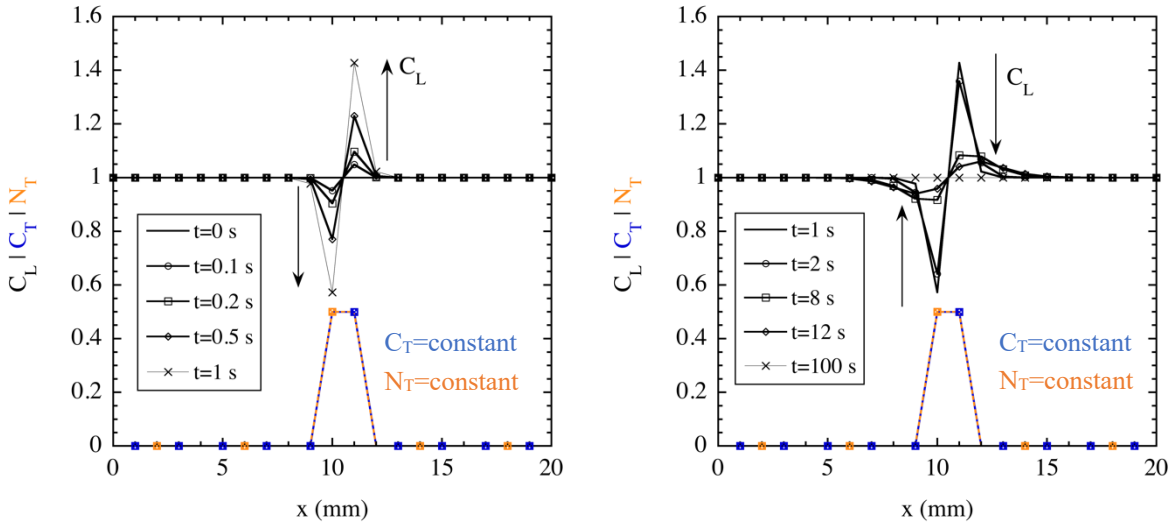

Figure 5. Repartition of C_L, C_T and N_T along the bar for different times: (a) accounting the extra term $\boldsymbol{\varphi}_d$ proposed by Dadfarnia [29] for $t \in [0s, 1s]$, and (b) supressing $\boldsymbol{\varphi}_d$ for $t \in [1s, 100s]$.

This last point consists in the main difference between the current approach and the one recently proposed by Dadfarnia [29] (see equations (7) and (8)).

In Figure 5a is presented the system evolution when considering the $\boldsymbol{\varphi}_d$ contribution. As it can be seen, the trap and trapped hydrogen concentration are not affected by $\boldsymbol{\varphi}_d$, controversy to C_L repartition.

At $t = 1\ s$, the $\boldsymbol{\varphi}_d$ term is disactivated, and the corresponding system evolution is plotted in Figure 5b: C_L return to its initial states due to the Fickian flux term $\boldsymbol{\nabla} C_L$. In the whole process, neither C_T nor N_T have been modified.

3 Validation of the TTD equation set

In the following, the TTD equation set is investigated in the reference Small Scale Yielding (SSY) configuration or the sake of comparison. This SSY configuration has been first defined by Sofronis & McMeeking in their study presenting the hydrogen transport and trapping equation [10], and then, has been used by several author for proposing their own modifications in this formalism to account for the effect of trap creation [11], transient trapping [18,49], boundary conditions [50,51], mechanical behavior [52-54], diffusive hydrogen flux modification [29], or just to validate a finite element implantation of the transport and trapping problem [55-57].

The main features of this configuration are first recalled, and the TTD implantation is then compared to bibliographic results for $D_T = 0$ mm^2/s (no dragging). It is worth noting that the results presented in [18] have been obtained by using a complete different implementation scheme, based especially on an approximation of the solution of the McNabb and Foster equation (see [43,58] for more details).

3.1 Configurations, mesh and boundary conditions

The studied configuration is a 2D Small Scale Yielding (SSY) one, under plane strain assumptions, as presented in Figure 6; this configuration is the same than in previous studies focused on the transport and trapping of hydrogen [10,11,18].

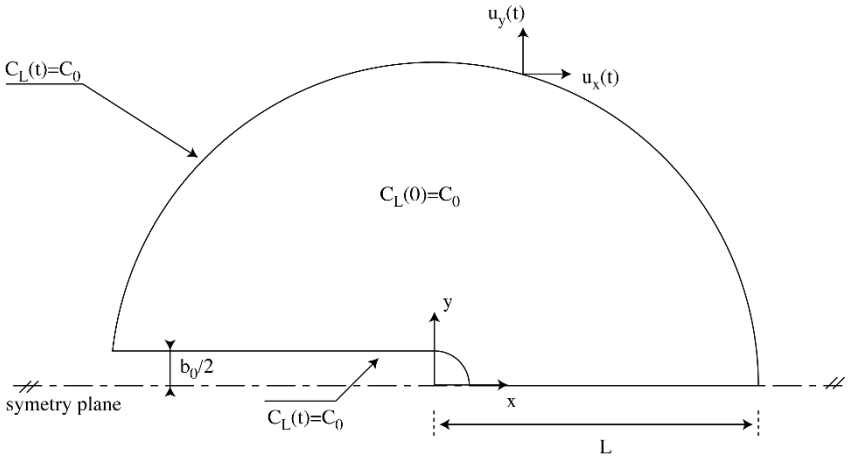

Figure 6. Geometrical configuration and boundary conditions for the application.

b_0 is set to 10 µm, L to 150 mm [11].

The system is mechanically loaded so that the stress field at the crack tip corresponds to a mode I loading whose stress intensity factor is equal to K_I, using u_x and u_y displacement functions so that [59]

$$\begin{cases} u_x = \dfrac{2(1+\nu)K_I}{2E}\sqrt{\dfrac{r}{2\pi}}\cos\dfrac{\theta}{2}\left(\kappa - 1 + 2\sin^2\dfrac{\theta}{2}\right) \\ u_y = \dfrac{2(1+\nu)K_I}{2E}\sqrt{\dfrac{r}{2\pi}}\sin\dfrac{\theta}{2}\left(\kappa + 1 - 2\cos^2\dfrac{\theta}{2}\right) \end{cases} \quad (19)$$

r et θ are the polar coordinates of the current point. K_I denotes the mode I stress intensity factor; last $\kappa = 3 - 4\nu$.

At $t = 0$, the system is assumed to be with no mechanical loadings, while $C_L = C_0$ and $N_T = 10^{20.93}$ m^{-3} (see below, equation (21)) are imposed everywhere. C_0 si set to 2.08×10^{21} m^{-3}, which corresponds to the hydrogen subsurface concentration induced by an exposition to a dihydrogen gas at 300 K and 1 atm [10]. The corresponding C_T value is computed based on the Oriani's equilibrium [18,19].

Thus, a mechanical loading is applied, with $\dot{K}_I = K_I/\tau$ characterizing its rate (τ being the loading time, and $K_I = 89.2$ MP$a\sqrt{m}$ [11]), while a constant diffusive hydrogen concentration $C_L = C_0$ is imposed on the outer surfaces except on the symmetry plane.

For $t > \tau$, the mechanical loading remains constant ($\dot{K}_I = 0$ MP$a\sqrt{m}$).

The sample is meshed using 1134 full integration 8-nodes tri-linear elements C3D8T, and structured to mimic the mesh used by [10].

3.2 Material parameters

The considered material is α-iron, with a mechanical behavior so that

$$\varepsilon = \begin{cases} \dfrac{\sigma}{E} \; if \; \varepsilon \leq \dfrac{\sigma_Y}{E} \\ \dfrac{\sigma_Y}{E}\left(\dfrac{\sigma}{\sigma_Y}\right)^n \; if \; \varepsilon \geq \dfrac{\sigma_Y}{E} \end{cases} \quad (20)$$

while the trap creation due to plastic strain is written as [10,12]

$$\log N_T = 23.26 - 2.33e^{-5.5\varepsilon_p} \quad (21)$$

where ε_p represents the equivalent plastic strain (N_T in trap/m^3). All of the needed parameters are extracted from [10,11] and are enlisted in Table 1.

Table 1. Parameters for α-iron.

D_L (m^2/s)	V_H (m^3)	E (GPa)	ν	σ_Y	n	N_L (m^{-3})	K_T	E_T (kJ)
1.27×10^{-8}	2×10^{-6}	207	0.3	250	5	5.1×10^{29}	5.04×10^{10}	60

Last, the p and k parameters of the trapping equation (5) are so that $k = K_T \times p$.

3.3 Results

A first set of computations have been performed to validate the implementation strategy proposed in section 2.2 and the TTD equation set.

First, results for an instantaneous trapping is checked by comparison with the reference work of Krom et al. [11], using τ=130 s and $p = 0.001\ s^{-1}$ (which is large enough to get an instantaneous trapping [18]).

Second, transient trapping, for various p values and $\tau = 1.3$ s, is investigated, by comparison with the results of Charles et al. [18].

Last, the computation of the trap density is verified, by comparing the results from the TTD equations (17)c and from the theoretical equation (21).

3.3.1 Mechanical fields and instantaneous trapping

The crack tip opening displacement at the end of the mechanical loading is equal to $b = 4.7b_0$, as in [10].

The evolution of the stress triaxiality and the diffusive hydrogen concentration along the crack path, at the end of the mechanical loading, are plotted in Figure 7a, while the repartition of C_L is plotted in Figure 7b.

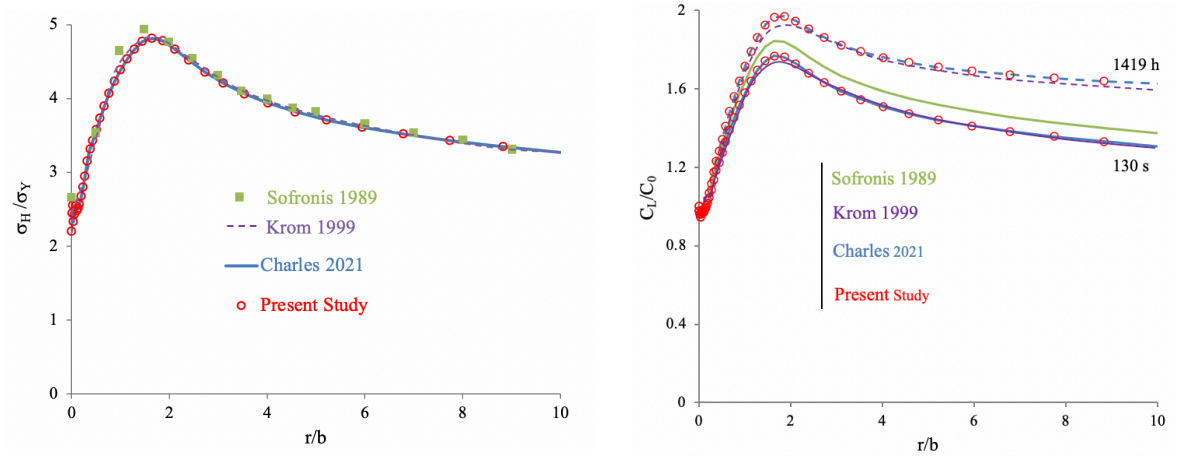

(a) (b)

Figure 7. Comparison of the repartition ahead of the crack tip of (a) the stress triaxiality at the end of the mechanical loading ($t = \tau$ =130 s) and (b) C_L at the end of the mechanical loading ($t = \tau$ =130 s) and at the end of the simulation (t =1419 h) ehead the crack tip ($\theta = 0$) as computed by Sofronis & McMeeking [10], Krom et al. [11], Charles et al. [18] and in the present study.

It can be seen that the proposed TTD equation set gives the same results than the one extracted from the literature, i.e., is able to model the hydrogen transport in strained structured and instantaneous (or very fast) trapping (and $D_T = 0$ mm^2/s).

3.3.2 Kinetic trapping

In Figure 8 are plotted the comparison between the normalized C_L repartition at the end of the mechanical loading for τ =1.3 s for different trapping kinetic, and computed using the scheme proposed by Benannoune et al. [43,58] on the one hand, and with the current implementation strategy on the second hand.

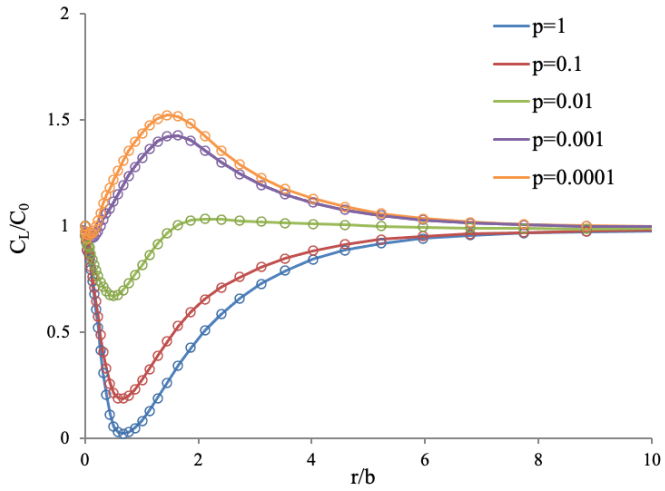

Figure 8. Comparison of the C_L repartition ahead the crack tip at the end of the mechanical loading ($t = \tau$ =1.3 s), for different trapping kinetic, computed with the proposed implementation strategy (open circle) and the one computed in [18] (full line).

The two approaches give the same results, and are consequently equivalent for $D_T = 0$ mm²/s.

3.3.3 Trap density evolution ($D_T = 0$ mm²/s)

In Figure 9 are plotted the evolution of the trap densities, computed by the TTD equation set (equation (17)c) and by the theoretical formulation given on equation (21). Two curves are presented: the variation of N_T with the equivalent plastic strain, and its evolution with time.

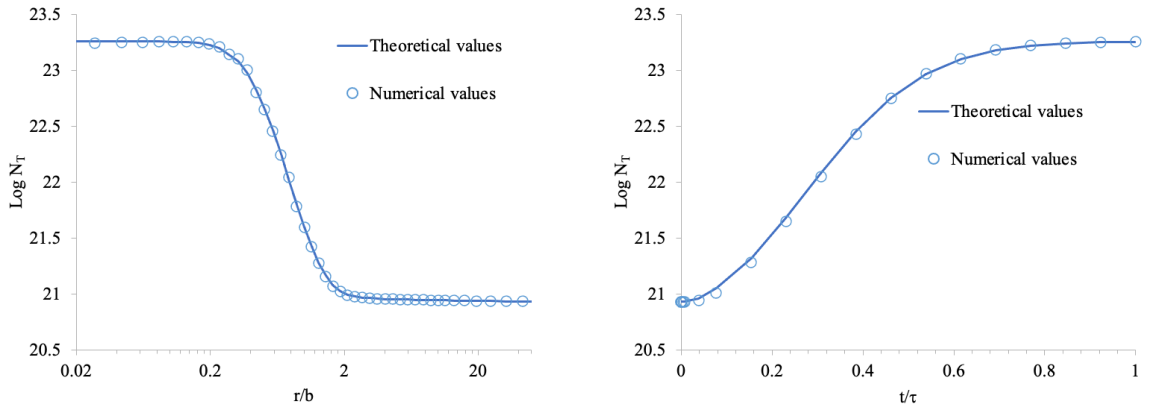

(a) (b)

Figure 9. Comparison of the reparitition of N_T (a) ahead the crack tip at the end of the mechanical loading ($t = \tau$) and (b) its evolution with time during loading, computed with the proposed implementation strategy (open circle) and equation (21) (full line) using the numerical equivalent plastic strain.

The superimposition of the curves leads to the conclusion that equations (21) and (17)c (for $D_T = 0$ mm²/s) are equivalent.

From the previous comparisons, the TTD equation set and the new implementation strategy is validated for immobile traps. As a consequence, the classically used approach the hydrogen transport and trapping modeling, and based on equation (1) and Oriani or McNabb and Foster trapping kinetic can be considered as a particular case of the TTD equation set.

In the following, the effect of trap mobility on hydrogen repartition is investigated.

4 Parametric study

The previous SSY configuration is used again and all the mechanical parameters and loading conditions are kept. Only the loading stage is considered, with $\dot{K}_I = K_I/\tau$.

Initially, the sample is set hydrogen-free (both diffusive and trapped), while $N_T = 10^{20.93}$ m^{-3}.

At $t = 0^+$, the mechanical loading is applied, at a constant $\dot{K}$, while insulated conditions are imposed on the outer surfaces (i.e., 0 normal flux) but on the crack, where $C_L = C_0$ is imposed.

The complete TTD equation set is used in the following, D_T being computed at each time, based on equation (15).

Hydrogen transport acceleration due to hydrogen dragging by mobile dislocation is investigated for two configurations:

- considering several loading time τ and a given trapping kinetic;
- considering the faster loadings and several trapping kinetics.

4.1 Influence on the loading time τ

In this section, τ varies from 0.0013 s to 130 s. Based on [18], p is set to 1 s^{-1} to get a fast trapping kinetic (for τ >1.3 s), keeping $k = K_T \times p$. In Figure 10 are plotted the repartition of C_L at the end of the mechanical loading ($t = \tau$) for $D_T \neq 0$ and $D_T = 0$.

The effect of non-zero D_T can be seen for all τ except for 130 s and 13 s: the C_L diffusion ahead the crack tip is faster due to trapped hydrogen dragging by mobile dislocation.

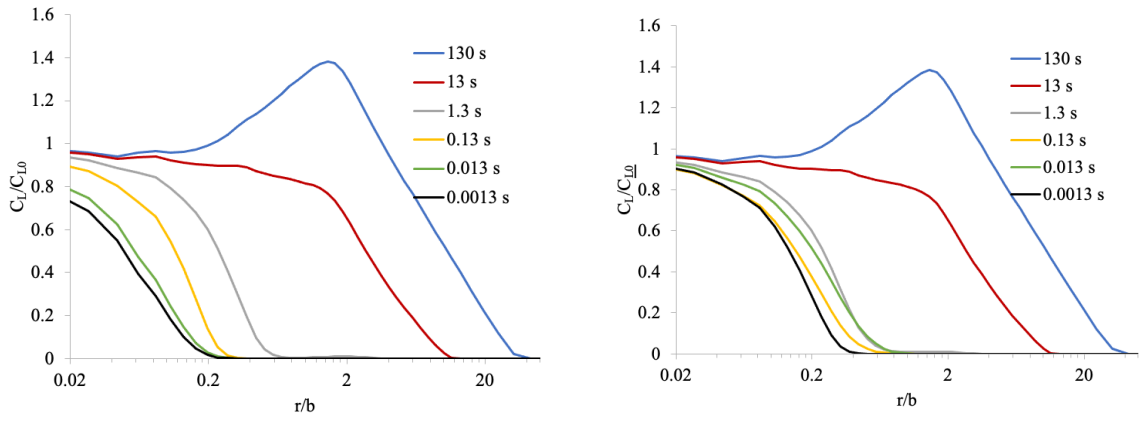

(a) $D_T = 0$mm^2/s (b) $D_T \neq 0$mm^2/s

Figure 10. Comparison of the C_L repartition ahead the crack tip at the end of the mechanical loading ($t = \tau$).

This acceleration can be better seen in Figure 11 on which the diffusion front location ratio at $t = \tau$ are plotted as a function of the load rate $\dot{K}_I$. The diffusion front is defined as the point where $C_L = 0.02C_{L0}$.

For $\tau \geq 13$ s, hydrogen dragging by mobile dislocation has no effect on the diffusion front location. The hydrogen transport acceleration appears for $\tau < 13$, and increases when τ decrease, until reaching a maximal value (around $\tau = 0.013$ s). For smaller τ -higher strain rates-, this acceleration decreases.

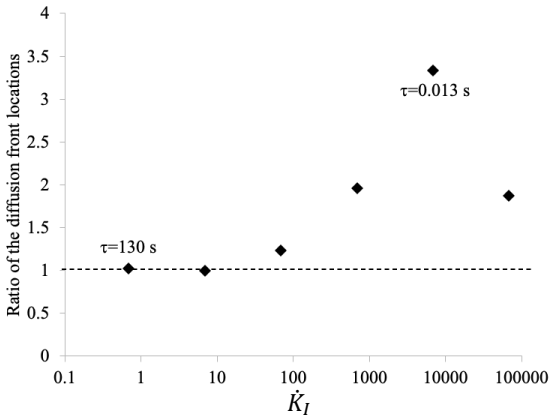

Figure 11. Acceleration of the apparent diffusion for several values for τ, and $p = 1\ s^{-1}$.

The increasing acceleration of hydrogen transport with decreasing time τ (>0.0013 s) -or increasing loading rate- illustrates the competition between diffusive hydrogen mobility and the conjunction of trap mobility and detrapping kinetic, respectively characterized by $D_L = 0.0127$ mm^2/s and D_T (which is plotted in Figure 12 for $\dot{\bar{\varepsilon}}_p = 1$ s^{-1}).

Two situations can be observed:

- if traps diffuse faster than mobile hydrogen ($\tau \leq 1.3$ s), thus, trapped hydrogen can be dragged ahead the diffusion front. The detrapping process leads then to the apparition of diffusive hydrogen ahead the diffusion front, inducing an apparent acceleration of the hydrogen transport process.
- if trap mobility is slower than the diffusive hydrogen's one, then, trapped hydrogen remains behind the diffusion front, and no acceleration of hydrogen transport can be observed ($\tau \geq 13$ s).

This observation can be linked to the relative D_L and D_T values:

- for τ =13 s, the maximal $\dot{\bar{\varepsilon}}_p$ value can be extracted from computations and is found equal to 0.137 s^{-1} (for τ =130 s, this latter is equal to 0.0137 s^{-1}), which is consistent with [29] (in which τ =8920 s leads to a maximal $\dot{\bar{\varepsilon}}_p$ value equal to 2x10^{-4} s^{-1}), leading to a maximal D_T value equal to 0.0257 mm^2/s (for $\bar{\varepsilon}_p$ =0%) which quickly decreases when $\bar{\varepsilon}_p$ increases (D_T=0.000274 mm^2/s for $\bar{\varepsilon}_p$ =10%). The mobile hydrogen diffuses then faster than traps: trap hydrogen dragging by dislocation has thus no influence on the diffusion front location.
- for τ =1.3 s, the maximal D_T value is 2.57 mm^2/s for $\bar{\varepsilon}_p$ =0%, and its value decreases toward 0.0257 mm^2/s for $\bar{\varepsilon}_p$ =10%. Traps are thus much more mobile than diffusive hydrogen, and trapped hydrogen is then likely to be transport ahead the diffusion front, thus accelerating the global hydrogen transport process once detrapping has occurred.

From the previous scenario, it could have been expected a continuous acceleration of hydrogen transport, as D_T increased when the loading time τ decrased. This is however not what it can be observed for τ =0.0013 s. This heterodox result is investigated in the next section.

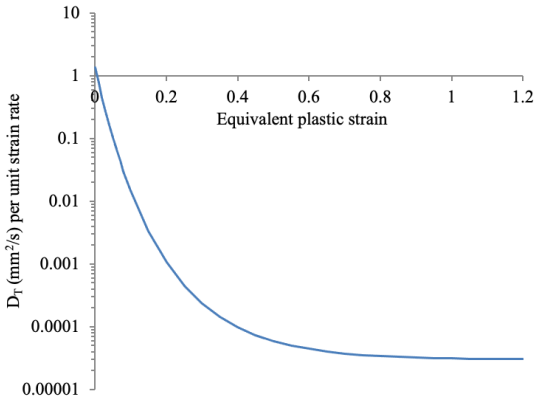

Figure 12. D_T evolution with $\bar{\varepsilon}_p$, for $\dot{\bar{\varepsilon}}_p$=1 s^{-1}.

In Figure 13 are plotted the repartition of the trapped hydrogen concentration ahead of the crack tip at the end of the mechanical loading ($t = \tau$) for different loading rates, considering or not trap mobility.

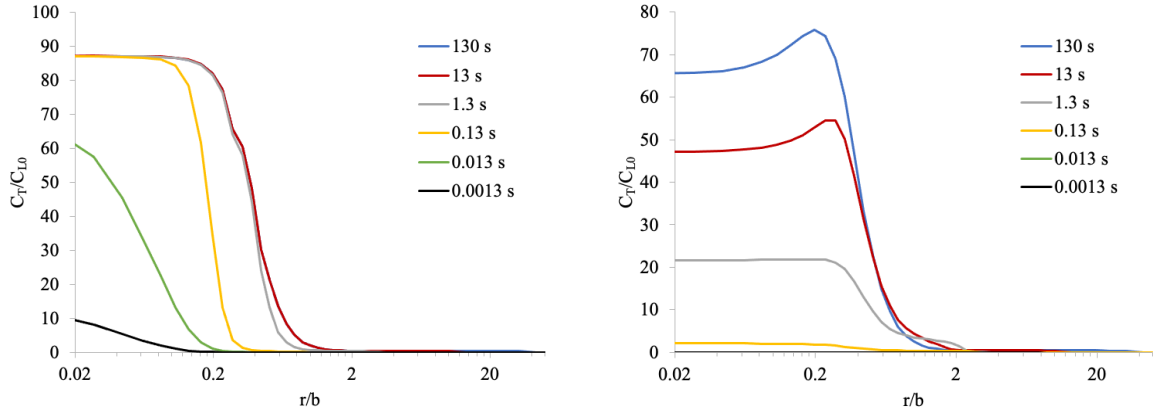

(a) $D_T = 0$ mm^2/s (b) $D_T \neq 0$ mm^2/s

Figure 13. Comparison of the C_T repartition ahead the crack tip at the end of the mechanical loading ($t = \tau$).

The C_T repartition plotted in Figure 13a is consistent with the trap repartition for $D_T = 0$ mm^2/s at $t = \tau$ (see Figure 9), considering the trapping kinetic effect. For important τ values ($\tau \geq 0.13$ s), the maximum value for C_T meets the N_T repartition: the trapping kinetic is fast enough to be considered as instantaneous: any increase in N_T induces a related increase in C_T (see [18]), keeping the trap occupancy θ_T constant. As soon as the loading rate increases (i.e., τ decreases), the trapping process can no longer be assimilated to an instantaneous one, and new traps created by plastic strain cannot be filled by hydrogen: the increase of N_T is thus more important than the increase of C_T, as it can be observed in Figure 13a.

For $D_T \neq 0$ mm^2/s (Figure 13b), it can be observed that the maximal C_T value is no longer at the crack tip but located 0.2-0.3r/b ahead. This is due to hydrogen dragging by mobile dislocations. This dragging is all the more important as τ decreases, leading to the acceleration of the hydrogen diffusion observed in Figure 11.

4.2 Influence on the trapping kinetic

To analyze the decrease of the hydrogen front acceleration for τ =0.0013 s, two loading times are here considered: τ =0.013 s and τ =0.0013 s, while the trapping kinetic evolves from a very slow mechanism (p=0.0001 s^{-1}) to an instantaneous one (p=1000 s^{-1}), with $k = K_T \times p$. Results are presented therafter.

4.2.1 Loading time τ equal to 0.013 s

In Figure 14 are plotted the repartition of the mobile hydrogen concentration C_L ahead of the crack tip, at the end of the loading time ($t = \tau$), for several p values.

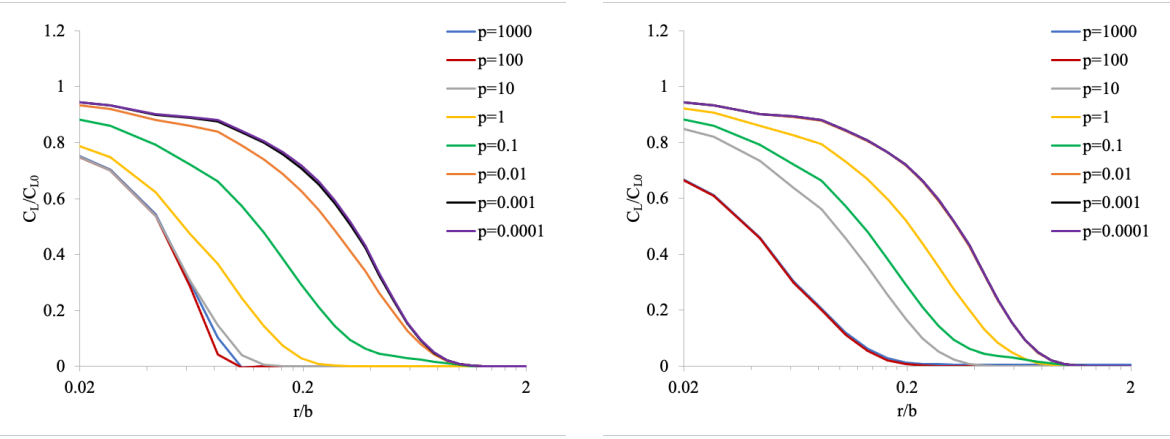

(a) $D_T = 0$ mm²/s (b) $D_T \neq 0$ mm²/s

Figure 14. Comparison of the C_L repartition ahead the crack tip at the end of the mechanical loading ($t = \tau = 0.013\ s$) for different traping kinetic ($k = K_T \times p$).

The acceleration of hydrogen transport can be seen for high p values, while, for the lower ones, hydrogen dragging by mobile dislocation seems to have no influence.

In Figure 15 is plotted the acceleration of the hydrogen transport versus p. For slow trapping kinetic, there is no acceleration: as the diffusive hydrogen is too slow to be trapped, mobile traps are mainly trapped hydrogen-free. When trapping becomes faster, trap tend to be filled, and thus trapped hydrogen is transported ahead the diffusion front, being then detrapped if the C_L value is low enough (following equation (17)d): the diffusion front accelerates. This acceleration is all the more important that the detrapping is slow, the traps being able to move further away from the diffusion front. An instantaneous trapping, on the contrary, leads to a release of the trapped hydrogen as soon as the C_L concentration is low enough, i.e., juste after the front diffusion.

These contradictory effects of the trapping kinetic on the front diffusion acceleration are well represented in Figure 15: $p = 1$ s^{-1} induces the most important acceleration of the diffusion front.

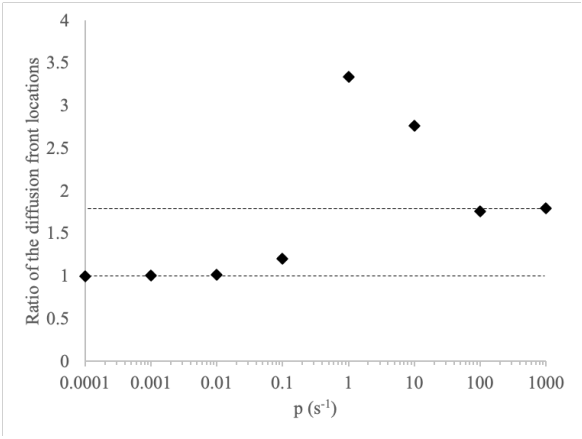

Figure 15. Acceleration of the hydrogen transport due to hydrogen dragging by mobile dislocation at the end of the mechanical loading ($t = \tau = 0.013\ s$) and for different traping kinetic ($k = K_T \times p$).

4.2.2 Loading time τ equal to 0.0013 s

The same computations have been conducted for τ =0.0013 s. In Figure 16 are plotted the C_L repartition ahead of the crack tip, at the end of the loading time ($t = \tau$), for several p values.

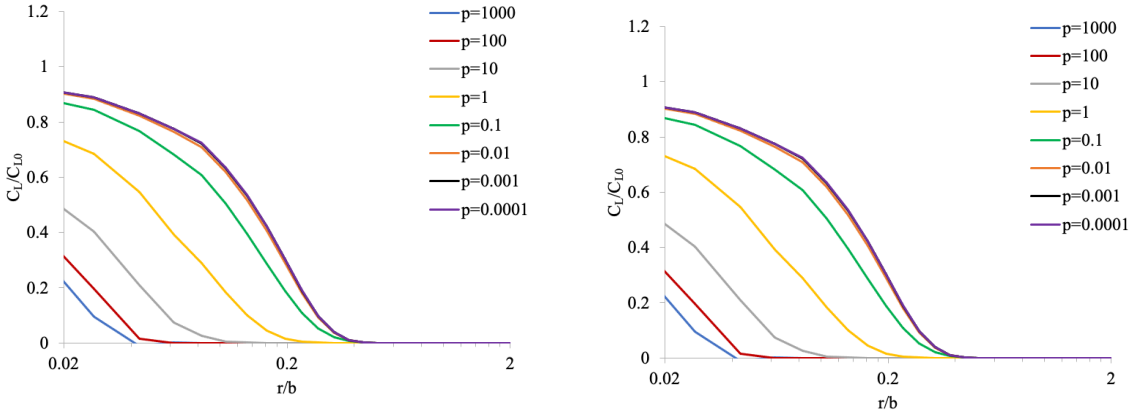

(a) $D_T = 0$ mm²/s (b) $D_T \neq 0$ mm²/s

Figure 16. Comparison of the C_L repartition ahead the crack tip at the end of the mechanical loading ($t = \tau = 0.0013\ s$) for different traping kinetic ($k = K_T \times p$).

As previously, the front diffusion acceleration depends on p, as illustrated in Figure 17: the acceleration apex appends for $p = 100$ s^{-1}. For $p = 1$ s^{-1}, there is quite no effect of hydrogen dragging on the diffusion front acceleration: therefore, the heterodox point in Figure 11 can be explained. If this point is replaced by the maximal value of Figure 17, the acceleration of the front diffusion with an increasing $\dot{K}_I$ becomes monotonous.

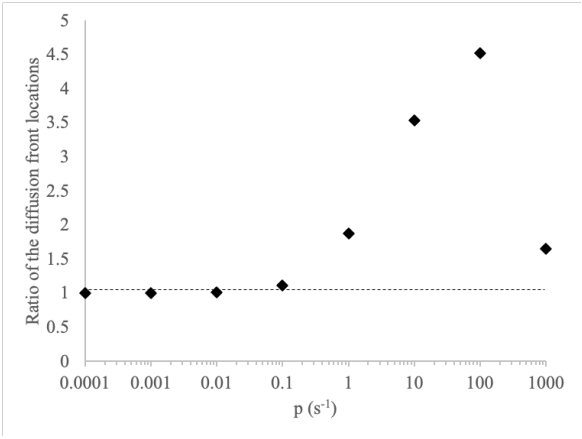

Figure 17. Acceleration of the hydrogen transport due to hydrogen dragging by mobile dislocation at the end of the mechanical loading ($t = \tau = 0.0013\ s$) and for different traping kinetic ($k = K_T \times p$).

To summarize this section, the TTD equation set has exhibited the competition between several mechanisms: hydrogen transport, hydrogen trapping (or detrapping), and trapped hydrogen dragging by mobile dislocation. When loading rate increases, hydrogen dragging becomes more and more important and the apparent hydrogen diffusion coefficient increases. However, apparent hydrogen diffusion is also dependent on the detrapping kinetic, as a too fast detrapping limits hydrogen apparent transport kinetic.

5 Dislocation breakaway from their hydrogen Cottrell atmosphere

Trapped hydrogen atoms around dislocation are also referred as hydrogen Cottrell atmosphere, following the work of [60], dealing with the interactions between solute atoms and a dislocation in motion. [61] pointed out that, for a critical dislocation velocity, the dragging force exerted by the dislocation to the Cottrell atmosphere reaches a maximum value: trapped hydrogen dragging by mobile dislocations no longer appends, leading to a release of these atoms, which become diffusive ones.

This phenomenon can be integrated in the modeling proposed in the current study, by modifying the trapping kinetic equation (17)d.

5.1 Modeling assumptions

As stated previously, the loss of the Cottrell atmosphere appends as soon as a dislocation velocity is greater than a critical value [20]

$$v \geq v_c \tag{22}$$

where

$$v_c = \frac{D_L}{RT}\frac{E_T}{30b} \tag{23}$$

From equation (11), it corresponds to a critical D_T value, so that

$$D_T \geq D_T^c = \frac{{v_c}^2}{2c} \tag{24}$$

For $D_T \geq D_T^c$, any trapped hydrogen must be released from the trap; this can be modeled by modifying equation (17)d as following

$$\frac{\partial C_T^r}{\partial t} = -\frac{\partial C_L^r}{\partial t} = \frac{k(D_T)}{N_L} C_L(N_T - C_T) - p(D_T)C_T \tag{25}$$

in which the trapping and detrapping rate constants p and k are set as D_T-dependant

$$p(D_T) = \begin{cases} p(0) \text{ if } D_T < D_T^c \\ +\infty \; if \; D_T \geq D_T^c \end{cases} \tag{26}$$

as well as the trapping one k

$$k(D_T) = \begin{cases} k(0) \text{ if } D_T < D_T^c \\ 0 \; if \; D_T \geq D_T^c \end{cases} \tag{27}$$

The equilibrium constant K_T thus evolves from $e^{-\Delta E_T/RT}$ to 0, meaning that, for $D_T \geq D_T^c$ no further trapping occurs, and, more, that all trapped hydrogen atoms are instantaneously released, whatever the trap density and the diffusive hydrogen concentration. In the following, for the sake of simplicity, p evolves from $p(0)$ to $100 \times p(0)$.

Using the parameters of the present study and equation (23), $v_c = 42$ m^2/s[2], unlikely to be reached for α-iron for the SSY configuration (i.e., $\dot{\bar{\varepsilon}}_p$ ≈2000 s^{-1} for $\bar{\varepsilon}_p$=0, or $\dot{\bar{\varepsilon}}_p$ ≈17000 s^{-1} for $\bar{\varepsilon}_p$=10%). For the sake of illustration, the value computed in [29] for fcc materials is used instead, i.e., $v_c = 10^{-7}$ m^2/s, leading to $D_T^c = 2.5 \times 10^{-5}$ mm^2/s.

5.2 Illustration

To illustrate the effect of dislocation breakaway from the hydrogen Cottrell modeling based on equation (25), the SSY configuration from of section 3.1 is considered, with the parameters enlisted on section 3.2 and $p = 1$ s^{-1} (i.e., instantaneous-like trapping kinetic).

The loading rate is set as follow:

$$\begin{cases} t \in [0{,}100], \dot{K}_I = 89.2/130 \; MPa\sqrt{m}/s \\ t \in [100{,}100 + 10^{-4}], \dot{K}_I = 89.2/0.0013 \; MPa\sqrt{m}/s \\ t \in [100 + 10^{-4}, 120 + 10^{-4}], \dot{K}_I = 89.2/130 \; MPa\sqrt{m}/s \end{cases} \tag{28}$$

and corresponds to a brutal acceleration as illustrated in Figure 18 (dotted line). It is worth noting that increasing the strain rate with a factor 10^5 leads to the same increase for D_T.

[2] v_c is equal to 53 m^2/s in [29] in which D_L =2×10^{-8} m^2/s and E_T=50 kJ are used, instead of the values enlisted in Table 1.

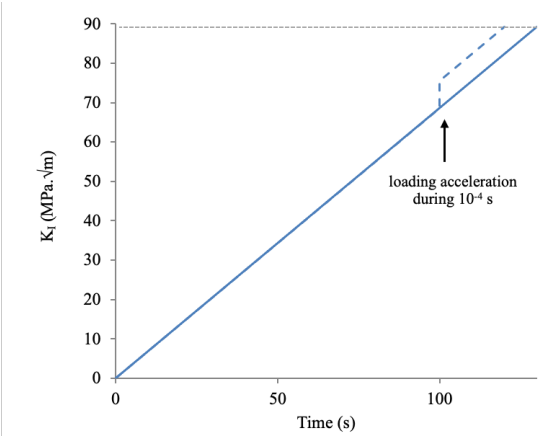

Figure 18. Loading configuration for illustrating hydrogen release from traps (dotted line), compared with the one used in the previous section (full line).

In Figure 19 are plotted the repartition of the diffusive hydrogen repartition ahead the crack tip at the end of the different loading steps ($t = 100$ s, $100 + 10^{-4}$ s and $120 + 10^{-4}$ s), considering different modeling assumptions (no trap mobility, trap mobility, and trap mobility plus trapped hydrogen released for $D_T \geq D_T^c$). For $t = 100$ s, no difference can be seen between the different modeling assumptions: $D_T \leq D_T^c$ at every sample point and at every time, and thus, trapped hydrogen repartition is not affected by trap mobility. At the end of the loading pulse, at $t = 100 + 10^{-4}$ s, trapped hydrogen release from fast moving dislocation induces an important increase of C_L. After resuming the initial loading rate, at $t = 120 + 10^{-4}$ s, all repartitions are superimposed: trapping kinetic is fast enough to reach equilibrium between C_L and C_T.

It is worth noting that, for all these steps, there is no difference between the effect C_L repartition computed by assuming no trap mobility or trap mobility only. This is expected because all the traps are filled ahead the crack tip ($\theta_T \approx 1$): trapped hydrogen dragging by mobile dislocation has no effect C_L repartition (see section 2.3).

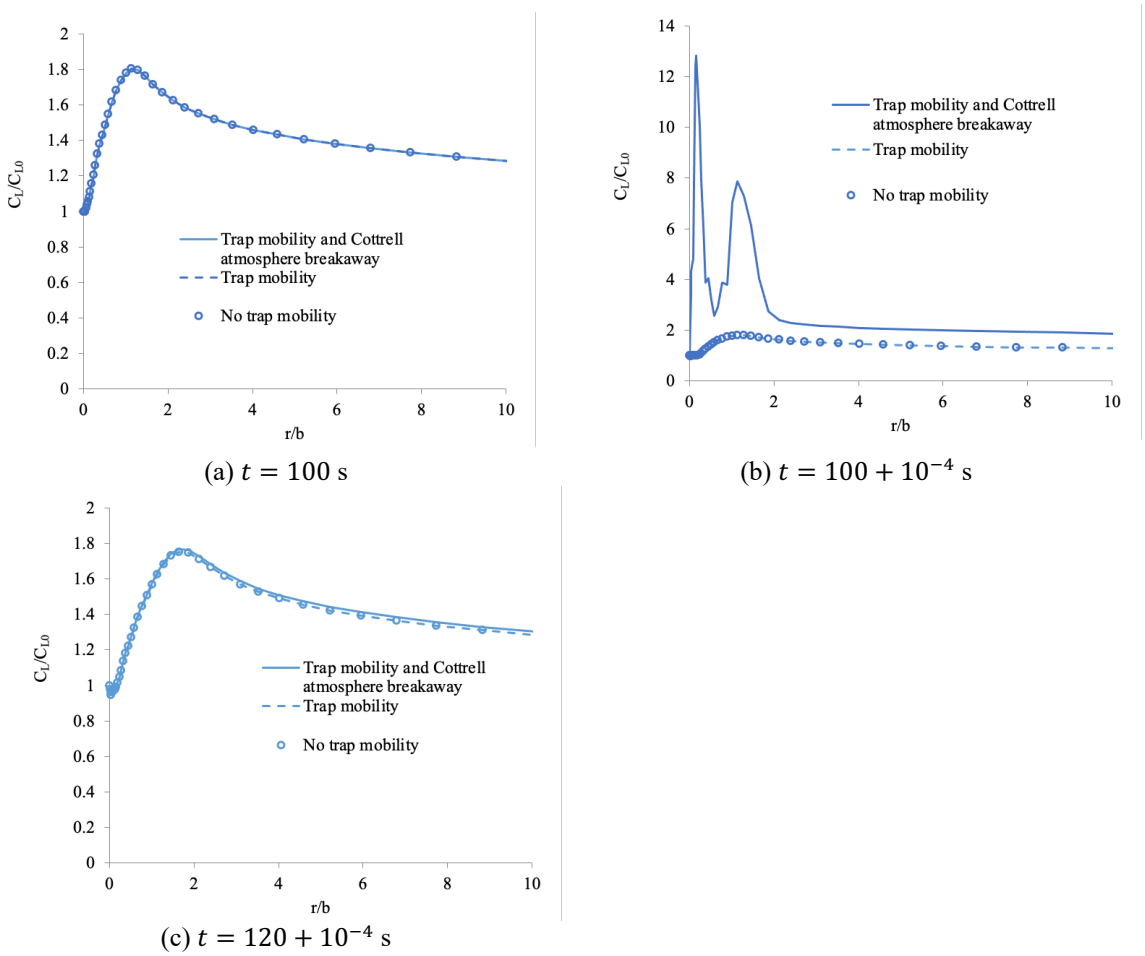

(a) $t = 100$ s

(b) $t = 100 + 10^{-4}$ s

(c) $t = 120 + 10^{-4}$ s

Figure 19. Evolution of the C_L repartition ahead the crack tip at the end of each loading steps (equation (28)) and considering trap mobility and trapped hydrogen released for $D_T \geq D_T^c$, trap mobility only, and the reference configuration (no trap mobility, $D_T = 0$ mm^2/s).

In Figure 20 are plotted the corresponding C_T repartition at the end of the three loading steps. The traps are very little filled at the end of the loading pulse, illustrating the dislocation breakaway for their Cottrell atmosphere for high enough loading rate. The rate of trapped hydrogen release depends on the value of p, and the detrapping kinetic is illustrated in Figure 21, on which are plotted the evolution of C_L and C_T with K_I, at $r/b = 0.16$, i.e., where the C_T is maximum (see Figure 19b).

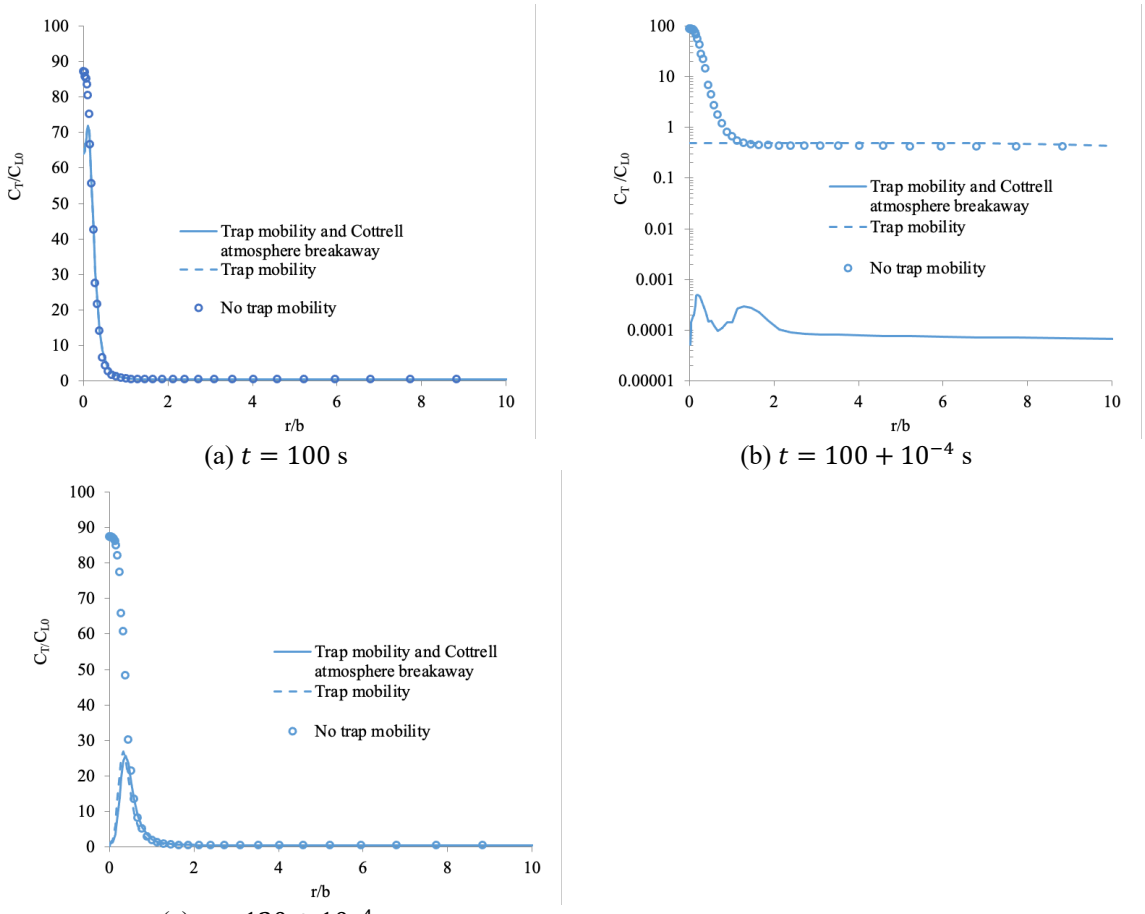

(a) $t = 100$ s (b) $t = 100 + 10^{-4}$ s

(c) $t = 120 + 10^{-4}$ s

Figure 20. Evolution of the C_L repartition ahead the crack tip at the end of each loading steps (equation (28)) and considering trap mobility and trapped hydrogen released for $D_T \geq D_T^c$, trap mobility only, and the reference configuration (no trap mobility, $D_T = 0$ mm^2/s).

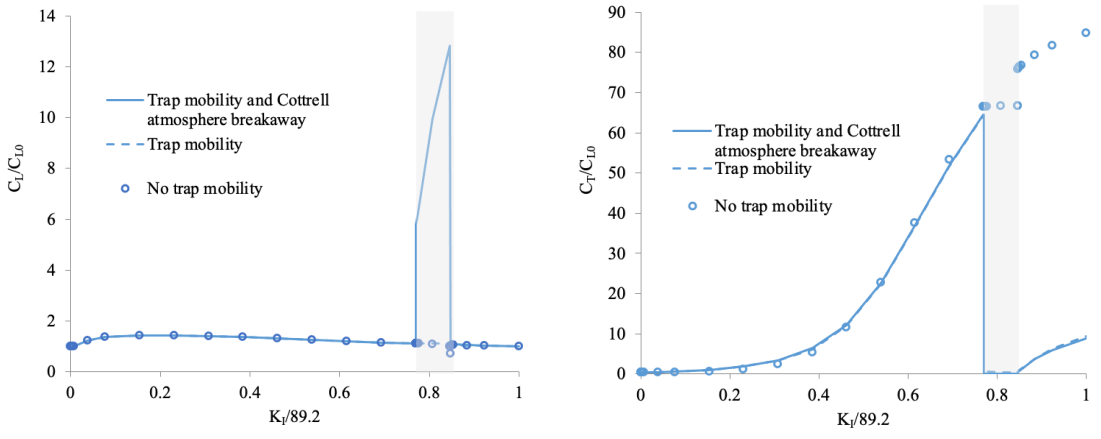

(a) (b)

Figure 21. Evolution with K_I of the (a) diffusive and (b) trapped hydrogen concentration near the crack tip, for different modeling assumptions. The grey square represents the loading pulse.

It can be indeed observed that the diffusive hydrogen concentration quickly increases at the beginning of the loading pulse, while the trapped hydrogen concentration decreases.

6 Conclusion

In this study, hydrogen dragging by mobile dislocations has been investigated and a modeling equation set based on specific multi-diffusion features has been proposed and applied on a reference SSY configuration.

This Transport, Trapping and Dragging (TTD) equation set is a generalization of the classical hydrogen transport and trapping equation and consequently leads to the same results than already published studies based an instantaneous or a kinetic trapping.

A parametric study has been conducted with the proposed equation set to investigate the condition of an apparent hydrogen acceleration and it has been shown that this apparent acceleration is maximum if the trapping is not instantaneous denoting the competition between several characteristic times (hydrogen diffusion, mechanical loading, trapping, trap mobility).

Last, the TTD framework has been shown to be flexible enough to allow the inclusion of the dislocation breakaway from their Cottrell atmosphere and illustrated on a loading pulse.

This work paths the way to further development in hydrogen-metal interactions, as trapping and dragging by vacancy or vacancy clusters, based on the same approach (see, e.g., [34]). Accounting for the effect of hydrogen on trap mobility is also a possible extension of that work and this approach, as including thermal effects. Development of Finite Element simulations accounting for various hydrogen-related mechanisms permits to supply powerful tools to improve prevention of hydrogen embrittlement for applications of great actuality at present, provided that experimental data are available.

Acknowledgements

This work has been carried out within the framework of the EUROfusion Consortium, funded by the European Union via the Euratom Research and Training Programme (Grant Agreement No 101052200 — EUROfusion). Views and opinions expressed are however those of the author(s) only and do not necessarily reflect those of the European Union or the European Commission. Neither the European Union nor the European Commission can be held responsible for them.

Bibliography

[1] ISO 11114-4. Transportable gas cylinders – compatibility of cylinder and valve materials with gas contents – part 4: test methods for selecting metallic materials resistant to hydrogen embrittlement., 2005.

[2] ASTM. Standard Practice for Making and Using U-Bend Stress-Corrosion Test Specimens, 2003.

[3] Juan A, Pistonesi C, García AJ, Brizuela G. The electronic structure and bonding of a H–H pair in the vicinity of a BCC Fe bulk vacancy. Int J Hydrog Energy 2003;28:995–1004. doi:10.1016/S0360-3199(02)00168-4.

[4] Djukic MB, Sijacki Zeravcic V, Bakic GM, Sedmak A, Rajicic B. Hydrogen damage of steels: A case study and hydrogen embrittlement model. Eng Fail Anal 2015;58:485–98. doi:10.1016/j.engfailanal.2015.05.017.

[5] Charles Y, Gaspérini M, Disashi J, Jouinot P. Numerical modeling of the Disk Pressure Test up to failure under gaseous hydrogen. J Mater Process Technol 2012;212:1761–70. doi:10.1016/j.jmatprotec.2012.03.022.

[6] Moriconi C, Hénaff G, Halm D. Cohesive zone modeling of fatigue crack propagation assisted by gaseous hydrogen in metals. Int J Fatigue 2014;68:56–66. doi:10.1016/j.ijfatigue.2014.06.007.
[7] Olden V, Thaulow C, Johnsen R, Østby E. Application of hydrogen influenced cohesive laws in the prediction of hydrogen induced stress cracking in 25% Cr duplex stainless steel. Eng Frac Mech 2008;75:2333–51. doi:10.1016/j.engfracmech.2007.09.003.
[8] Kumnick AJ, Johnson HH. Hydrogen transport through annealed and deformed armco iron. Met Trans A 1974;5:1199–206. doi:10.1007/BF02644334.
[9] Lufrano J, Sofronis P. Enhanced hydrogen concentrations ahead of rounded notches and cracks—competition between plastic strain and hydrostatic stress. Acta Mater 1998;46:1519–26. doi:10.1016/S1359-6454(97)00364-9.
[10] Sofronis P, McMeeking RM. Numerical analysis of hydrogen transport near a blunting crack tip. J Mech Phys Solids 1989;37:317–50. doi:10.1016/0022-5096(89)90002-1.
[11] Krom AHM, Koers RWJ, Bakker AD. Hydrogen transport near a blunting crack tip. J Mech Phys Solids 1999;47:971–92. doi:10.1016/S0022-5096(98)00064-7.
[12] Kumnick AJ, Johnson HH. Deep trapping states for hydrogen in deformed iron. Acta Metall 1980;28:33–9. doi:10.1016/0001-6160(80)90038-3.
[13] Li JCM, Oriani RA, Darken LS. The Thermodynamics of Stressed Solids. Z Phys Chem 1966;49:271–90. doi:10.1524/zpch.1966.49.3_5.271.
[14] Dederichs PH, Schroeder K. Anisotropic diffusion in stress fields. Phys Rev B 1978;17:2524–36. doi:10.1103/PhysRevB.17.2524.
[15] Bogkris JO, Beck W, Genshaw MA, Subramanyan PK, Williams FS. The effect of stress on the chemical potential of hydrogen in iron and steel 1971;19:1209–18. doi:10.1016/0001-6160(71)90054-X.
[16] Drexler A, Depover T, Leitner S, Verbeken K, Ecker W. Microstructural based hydrogen diffusion and trapping models applied to Fe–CX alloys. J Alloy Compd 2020;826:154057. doi:10.1016/j.jallcom.2020.154057.
[17] McNabb A, Foster PK. A new analysis of the diffusion of hydrogen in iron and ferritic steels. Trans Metall Soc AIME 1963;227:618–27.
[18] Charles Y, Mougenot J, Gaspérini M. Effect of transient trapping on hydrogen transport near a blunting crack tip. Int J Hydrog Energy 2021;46:10995–1003. doi:10.1016/j.ijhydene.2020.12.155.
[19] Oriani RA. The diffusion and trapping of hydrogen in steel. Acta Metall 1970;18:147–57. doi:10.1016/0001-6160(70)90078-7.
[20] Tien JK, Thompson AW, Bernstein IM, Richards RJ. Hydrogen transport by dislocations. Met Trans A 1976;7:821–9. doi:10.1007/BF02644079.
[21] Donovan JA. Accelerated evolution of hydrogen from metals during plastic deformation. Met Trans A 1976;7:1677–83. doi:10.1007/BF02817885.
[22] Albrecht J, Bernstein IM, Thompson AW. Evidence for Dislocation Transport of Hydrogen in Aluminum. Met Trans A 1982;13:811–20. doi:10.1007/BF02642394.
[23] Hirth JP, Johnson HH. On the Transport of Hydrogen by Dislocations. Atomistics of Fracture, vol. 232, Boston, MA: Springer US; 1983, pp. 771–87. doi:10.1007/978-1-4613-3500-9_26.
[24] Berkowitz BJ, Heubaum FH. Dislocation Transport of Hydrogen in Steel. In: Latanison RM, Pickens JR, editors. Atomistics of Fracture, vol. 10, Boston, MA: Springer US; 1983, pp. 823–7. doi:10.1007/978-1-4613-3500-9_31.
[25] Hwang C, Bernstein IM. Dislocation transport of hydrogen in iron single crystals 1986;34:1001–10. doi:10.1016/0001-6160(86)90209-9.

[26] Hwang C, Bernstein IM. The Fundamentals of Dislocation Transport of Hydrogen in BCC Iron. Pittsburgh: 1984.
[27] Abdelmawla A, Hatem TM, Ghoniem NM. Dislocation-Based Finite Element Modelling of Hydrogen Embrittlement in Steel Alloys. TMS 2018 147th Annual Meeting & Exhibition Supplemental Proceedings, vol. 196, Cham: Springer, Cham; 2018, pp. 213–23. doi:10.1007/978-3-319-72526-0_20.
[28] Frankel GS, Latanision RM. Hydrogen transport during deformation in nickel: Part II. Single crystal nickel. Met Trans A 1986;17:869–75. doi:10.1007/BF02643863.
[29] Dadfarnia M, Martin ML, Nagao A, Sofronis P, Robertson IM. Modeling hydrogen transport by dislocations. J Mech Phys Solids 2015;78:511–25. doi:10.1016/j.jmps.2015.03.002.
[30] Sills RB, Cai W. Solute drag on perfect and extended dislocations. Philos Mag 2016;96:895–921. doi:10.1080/14786435.2016.1142677.
[31] Krom AHM, Bakker AD. Hydrogen trapping models in steel. Metall Mater Trans B 2000;31:1475–82. doi:10.1007/s11663-000-0032-0.
[32] Charles Y, Nguyen TH, Ardon K, Gaspérini M. Scale Transition in Finite Element Simulations of Hydrogen–Plasticity Interactions. In: Ionescu I, Queyreau S, Picu C, Salman OU, editors. Mechanics and Physics of Solids at Micro- and Nano-Scales. 1st ed., Wiley; 2019, pp. 87–129. doi:10.1002/9781119687566.ch4.
[33] Zirkle T, Costello L, Zhu T, McDowell DL. Modeling Dislocation-Mediated Hydrogen Transport and Trapping in Fcc Metals. J Eng Mater Technol 2021. doi:10.1115/1.4051147.
[34] Ebihara K-I, Sugiyama Y, Matsumoto R, Takai K, Suzudo T. Numerical Interpretation of Hydrogen Thermal Desorption Spectra for Iron with Hydrogen-Enhanced Strain-Induced Vacancies. Metall Mater Trans A 2020;80:1–13. doi:10.1007/s11661-020-06075-7.
[35] Bammann DJ, Aifantis EC. On a proposal for a continuum with microstructure. Acta Mech 1982;45:91–121. doi:10.1007/BF01295573.
[36] Walgraef D, Aifantis EC. Dislocation patterning in fatigued metals as a result of dynamical instabilities. J Appl Phys 1985;58:688–91.
[37] Aifantis EC. On the dynamical origin of dislocation patterns. Mater Sci Eng A 1986;81:563–74. doi:10.1016/0025-5416(86)90293-4.
[38] Schiller C, Walgraef D. Numerical simulation of persistent slip band formation. Acta Metall 1988;36:563–74. doi:10.1016/0001-6160(88)90089-2.
[39] Aifantis EC. The physics of plastic deformation. Int J Plast 1987;3:211–47.
[40] Gordon PA, Neeraj T, Luton MJ. Atomistic simulation of dislocation nucleation barriers from cracktips in α-Fe. Model Simul Mater Sci Eng 2008;16:045006. doi:10.1088/0965-0393/16/4/045006.
[41] Lutts A, Gielen P, IUCr. The precise determination of the lattice parameter of α-iron and some of its alloys. J Appl Crystallogr 1971;4:242–50. doi:10.1107/S0021889871006770.
[42] Charles Y, Nguyen TH, Gaspérini M. FE simulation of the influence of plastic strain on hydrogen distribution during an U-bend test. Int J Mech Sci 2017;120:214–24. doi:10.1016/j.ijmecsci.2016.11.017.
[43] Benannoune S, Charles Y, Mougenot J, Gaspérini M. Numerical simulation of the transient hydrogen trapping process using an analytical approximation of the McNabb and Foster equation. Int J Hydrog Energy 2018;43:9083–93. doi:10.1016/j.ijhydene.2018.03.179.

[44] Charles Y, Gaspérini M, Fagnon N, Ardon K, Duhamel A. Finite element simulation of hydrogen transport during plastic bulging of iron submitted to gaseous hydrogen pressure. Eng Frac Mech 2019;218:106580. doi:10.1016/j.engfracmech.2019.106580.
[45] Benannoune S, Charles Y, Mougenot J, Gaspérini M, De Temmerman G. Multidimensional finite-element simulations of the diffusion and trapping of hydrogen in plasma-facing components including thermal expansion. Phys Scr 2020;T171:014011. doi:10.1088/1402-4896/ab4335.
[46] Vasikaran E, Charles Y, Gilormini P. Implementation of a reaction-diffusion process in the Abaqus finite element software. Mech Indus 2020;21:508. doi:10.1051/meca/2020010.
[47] Simulia. Abaqus User subroutines reference guide. Dassault Système; 2011.
[48] Charles Y. A finite element formulation to model extrinsic interfacial behavior. Finite Elem Anal Des 2014;88:55–66. doi:10.1016/j.finel.2014.05.008.
[49] Kanayama H, Ndong-Mefane S, Ogino M, Miresmaeili R. Reconsideration of the Hydrogen Diffusion Model Using the McNabb-Foster Formulation. Mem Fac Eng Kyushu Univ 2009;69:146–61.
[50] Turnbull A, Ferriss DH, Anzai H. Modelling of the hydrogen distribution at a crack tip. Mater Sci Eng A 1996;206:1–13.
[51] Martínez-Pañeda E, Díaz A, Wright L, Turnbull A. Generalised boundary conditions for hydrogen transport at crack tips. Corros Sci 2020:108698. doi:10.1016/j.corsci.2020.108698.
[52] Martínez-Pañeda E, Niordson CF, Gangloff RP. Strain gradient plasticity-based modeling of hydrogen environment assisted cracking. Acta Mater 2016;117:321–32. doi:10.1016/j.actamat.2016.07.022.
[53] Sasaki D, Koyama M, Higashida K, Tsuzaki K, Noguchi H. Effects of hydrogen-altered yielding and work hardening on plastic-zone evolution: A finite-element analysis. Int J Hydrog Energy 2015;40:9825–37. doi:10.1016/j.ijhydene.2015.05.187.
[54] Zhang B, Li S, Li Y. Numerical approach for predicting hydrogen diffusion in dual-phase hot stamped boron steel with hydrogen embrittlement. Journal of Materials Research and Technology 2021. doi:10.1016/j.jmrt.2021.10.041.
[55] Ndong-Mefane S, Kanayama H, Ogino M, El-Amin MF. A Stabilization Method for the Hydrogen Diffusion Model in Materials. J Comput Sci Tech-Ch 2008;2:447–58. doi:10.1299/jcst.2.447.
[56] Oh C-S, Kim YJ, Yoon KB. Coupled analysis of hydrogen transport using ABAQUS. J Solid Mech Mater Eng 2010;4:908–17. doi:10.1299/jmmp.4.908.
[57] Díaz A, Alegre JM, Cuesta II. Coupled hydrogen diffusion simulation using a heat transfer analogy. Int J Mech Sci 2016;115-116:360–9. doi:10.1016/j.ijmecsci.2016.07.020.
[58] Charles Y, Benannoune S, Mougenot J, Gaspérini M. Numerical simulation of the transient hydrogen trapping process using an analytical approximation of the McNabb and Foster equation. Part 2: Domain of validity. Int J Hydrog Energy 2021;46:30173–89. doi:10.1016/j.ijhydene.2021.06.138.
[59] Rice JR. Mathematical analysis in the mechanics of fracture. In: Liebowitz H, editor. Fracture: An Advanced Treatise, vol. 2, Fracture: an advanced treatise; 1968, pp. 191–311.
[60] Cottrell AH, Jaswon MA. Distribution of solute atoms round a slow dislocation. Proc R Soc Lond a Math Phys Sci 1949. doi:10.1098/rspa.1949.0128.
[61] Cottrell AH. Dislocations and Plastic Flow in Crystals. New York: Oxford University Press; 1953.